Surface second-harmonic generation from coupled spherical plasmonic nanoparticles: Eigenmode analysis and symmetry properties

Jérémy Butet,* Shourya Dutta-Gupta, and Olivier J. F. Martin
Nanophotonics and Metrology Laboratory (NAM), Swiss Federal Institute of Technology Lausanne (EPFL), 1015, Lausanne, Switzerland
(Received 9 May 2014; revised manuscript received 18 June 2014; published 30 June 2014)

The surface second-harmonic generation from interacting spherical plasmonic nanoparticles building different clusters (symmetric and asymmetric dimers, trimers) is theoretically investigated. The plasmonic eigenmodes of the nanoparticle clusters are first determined using an *ab initio* approach based on the Green's functions method. This method provides the properties, such as the resonant wavelengths, of the modes sustained by a given cluster. The fundamental and second-harmonic responses of the corresponding clusters are then calculated using a surface integral method. The symmetry of both the linear and nonlinear responses is investigated, as well as their relationship. It is shown that the second-harmonic generation can be significantly enhanced when the fundamental field is such that its second harmonic matches modes with suitable symmetry. The role played by the nanogaps in second-harmonic generation is also underlined. The results presented in this article demonstrate that the properties of the second-harmonic generation from coupled metallic nanoparticles cannot be fully predicted from their linear response only, while, on the other hand, a detailed knowledge of the underlying modal structure can be used to optimize the generation of the second harmonic.

DOI: 10.1103/PhysRevB.89.245449 PACS number(s): 78.67.Bf, 42.65.Ky, 73.20.Mf

I. INTRODUCTION

Plasmonic nanostructures play an important role in the current development of applications in nanophotonics [1]. These nanostructures have unique and interesting optical properties thanks to the surface plasmon resonances they support [2]. These resonances are associated with strong scattering, absorption, as well as localization of light far below the diffraction limit [3]. Spherical metallic nanoparticles are ideal systems for studying their properties, such as the resonance wavelength or width [4]. Indeed, the interaction between a plasmonic nanosphere and an electromagnetic excitation plane wave can be handled analytically using a multipole expansion deduced from Mie theory [4]. This theory predicts the influence of the surrounding medium, of the nanoparticle diameter, and of the chemical composition, on the surface plasmon resonance properties. Unfortunately, the surface plasmon resonances sustained by nanospheres are weakly tunable; i.e., they are difficult to adjust for practical applications such as refractive index sensing [5,6], surface-enhanced Raman spectroscopy [7], and single molecule detection [8,9]. It is however possible to overcome this limitation by using the coupling between plasmonic modes supported by several particles [10]. Indeed, the plasmonic modes supported by individual nanoparticles hybridize when the nanoparticles are moved close to each other [11]. A simple example of interacting plasmonic systems is just two nanoparticles forming a nanodimer [12,13]. The properties of the plasmon resonance of such a dimer, for example, the resonance wavelength, not only depend on the nanoparticles' diameters or their chemical composition, but also on the spacing between the nanoparticles [14,15]. This dependence allows for the design of a nanoruler based on the resonance shift induced by a modification of the gap distance [15]. Furthermore, new optical features, such as Fano resonances arising from the coupling between modes with different radiative properties [16–19], are observed when nanoparticles interact. The number of modes, and then the complexity of the optical response, increases with the number of constituent nanoparticles. The optical properties of nanotrimers [19,20], quadrumers [21,22], and heptamers [23] have been intensively studied as examples of clusters with particular symmetry, and the point group theory provides a clear insight into the hybridized mode properties [18,24,25]. While the linear optical properties of nanoparticle cluster are now well understood, this is not the case for their nonlinear response. The role played by plasmon modes in the enhancement of nonlinear optical processes such as second-harmonic generation (SHG) [26–29], third-harmonic generation [30,31], and four-waves mixing [32] is a key factor in the development of promising applications such as nonlinear optical sensing [33,34], nonlinear optical characterization [35–37], and nonlinear imaging [38,39]. As a consequence, the development of suitable theoretical tools to understand how this enhancement occurs is important [40–47]. While the nonlinear optical response of complex nanoclusters can be numerically evaluated [48–51], the role played by each individual plasmon mode is difficult to assess using such numerical methods [52]. Hence, it is difficult to obtain a description of the nonlinear response of a plasmonic cluster in terms of its underlying modal structure, which is important for optimizing its nonlinear response [53,54].

In this article, SHG from interacting spherical plasmonic nanoparticles is theoretically investigated, and an *ab initio* approach based on the Green's functions method is used to determine the eigenmodes of plasmonic clusters. The fundamental and second-harmonic (SH) responses of the corresponding clusters are then calculated using a surface integral equation (SIE) method. Combining both methods reveals the role played by the different eigenmodes in the SHG at both the excitation and the reemission steps, as well as their relation with the cluster symmetry. Several cluster geometries are considered, namely, symmetric/asymmetric dimers and linear trimers.

*jeremy.butet@epfl.ch

II. THEORETICAL METHODS

A. Eigenmode evaluation of plasmonic systems

The eigenmodes of the plasmonic system are calculated using a method based on the Green's tensor [55]. We consider a system composed of n spherical particles and assign to each particle a dipole. This approximation is valid when the size of the particle is much smaller than the effective wavelength in the material; for plasmonic nanostructures at optical frequencies, this holds for particles smaller than about 50 nm [4]. For larger nanostructures, the same approach can be used, but the different nanostructures must be split into a collection of dipoles [56]. The electric field due to a discretized system composed of n dipoles can be computed as

$$\vec{E}_i = \vec{E}_i^0 + \sum_{j=1, j\neq i}^{n} \overleftrightarrow{G}_{ij} \cdot k_0^2 \Delta\varepsilon_j V_j \vec{E}_j + \overleftrightarrow{M}_i \cdot \Delta\varepsilon_i \vec{E}_i - \overleftrightarrow{L} \cdot \vec{E}_i, \tag{1}$$

where $\vec{E}_i$ represents the total, self-consistent, electric field, $\vec{E}_i^0$ is the incident field, $\overleftrightarrow{G}_{ij}$ is the homogeneous Green's tensor, $\overleftrightarrow{M}_i$ is the self-term, $\overleftrightarrow{L}$ is the depolarization, $\Delta\varepsilon = (\varepsilon_i - \varepsilon_B)$ is the dielectric function contrast with the background, and V_j is the volume of the particle [55]. Equation (1) can be written into a matrix form,

$$(\overleftrightarrow{1} - \overleftrightarrow{S}) \cdot \vec{E} = \vec{E}_0, \tag{2}$$

where the right-hand side contains information about the incident condition, and the left-hand side contains the information on the structure, i.e., the matrix $\overleftrightarrow{S}$; $\overleftrightarrow{1}$ is the unit matrix. In order to evaluate the eigenmodes, we determine the possible field distributions when the incident field is zero, i.e., when the right-hand side of the equation is a null column vector. In this case, Eq. (2) reduces to

$$(\overleftrightarrow{1} - \overleftrightarrow{S}) \cdot \vec{E} = \vec{0}, \tag{3}$$

which must be solved to obtain the possible modes in the structure. Let $\xi_q(\omega)$, $q = 1,2,\ldots,3n$, where n is the number of dipoles, be the eigenvalues of the matrix $\overleftrightarrow{S}$ (we recall that we are dealing with a vectorial problem, where the three components of the electric field are associated with each dipole). Note that nonzero values of $\vec{E}$ are only found when $\xi_q(\omega_q) = 1$ for some $q = 1,2,\ldots,3n$. The corresponding frequencies ω_q are the eigenfrequencies of the system related to the eigenvectors of matrix $\overleftrightarrow{S}$, which give the field distributions for the respective eigenmodes. In practice, the eigenfrequencies are determined numerically by computing the eigenvalues of the matrix $\overleftrightarrow{S}$, ξ_q, in the parameter space of real and imaginary ω and identifying the points at which ξ_q is equal to 1. It should be noted that the matrix $\overleftrightarrow{S}$ depends both on the structure and the frequency ω. The dielectric function of gold is modeled using a modified Drude model taking into account the interband transitions [57]. The dielectric function is then given by

$$\varepsilon(\omega) = \varepsilon_\infty - \frac{\omega_p^2}{\omega^2 - i\gamma\omega} + I(\omega), \tag{4}$$

where the term $I(\omega)$ is the contribution of interband transitions to the dielectric function. The eigenvalue matrix equation does not have a solution if ω is purely real, and one needs to consider a complex value $\omega = \omega_r + i\omega_i$ for finding the eigenvalue [58]. Physically, the imaginary part of the eigenfrequency corresponds to the width of the plasmon resonance [58].

B. Surface integral equation method

The SHG computations have been performed using the SIE method reported in Ref. [49]. Note that this method has been recently extended to periodic nanostructures [59]. The SIE method for SHG is only briefly described here, and the reader is referred to previous publications for the numerical implementation details [49,59]. The linear surface currents, which are expanded on Rao-Wilton-Glisson (RWG) basis functions [60,61], are used for the evaluation of the fundamental electric fields just below the gold surfaces and then used for the calculation of the surface SH polarization. Only the component $\chi_{S,\perp\perp\perp}$ of the surface tensor, where $_\perp$ denotes the component normal to the surface, is considered, since recent experiments indicate that this term dominates the surface response of metallic nanoparticles [62]. Note that other contributions to the SH signal, namely, the component $\chi_{S,////\perp}$ of the surface tensor (where $_{//}$ denotes the component tangential to the surface), as well as bulk contribution, are theoretically allowed, but these contributions weakly contribute to the total SH response [62,63]. Furthermore, the present work is focused on the role played by the plasmon eigenmodes in the SHG enhancement from nanoparticle assemblies, and the following discussion is valid whatever the nonlinear sources. In the present case, only the normal component of the nonlinear polarization does not vanish, which can be written as

$$P_\perp(\vec{r},2\omega) = \chi_{S,\perp\perp\perp} E_\perp(\vec{r},\omega) E_\perp(\vec{r},\omega). \tag{5}$$

The SH surface currents are obtained by solving the SIE formulation, taking into account the nonlinear polarization and enforcing the boundary conditions at the nanostructure surfaces [64]. Like the linear surface currents, the SH surface currents are expanded on RWG basis functions. The expanding coefficients are found by applying the method of moments with Galerkin's testing [61]. A Poggio-Miller-Chang-Harrington-Wu formulation is used to ensure accurate solutions even at resonant conditions [61,65]. The SH electric field is then deduced from the SH surface currents using a singularity subtraction method for the evaluation of the Green's functions [61]. The surface of the plasmonic nanostructures is discretized with a triangular mesh with typical side of 2 nm (Fig. 1). Note that the discretization of the nanostructures is not required for the *ab initio* eigenmode analysis described above.

III. RESULTS AND DISCUSSION

In this section, the SHG from coupled metallic nanoparticles is investigated using the two methods described above: the *ab initio* method for the determination of the eigenmode

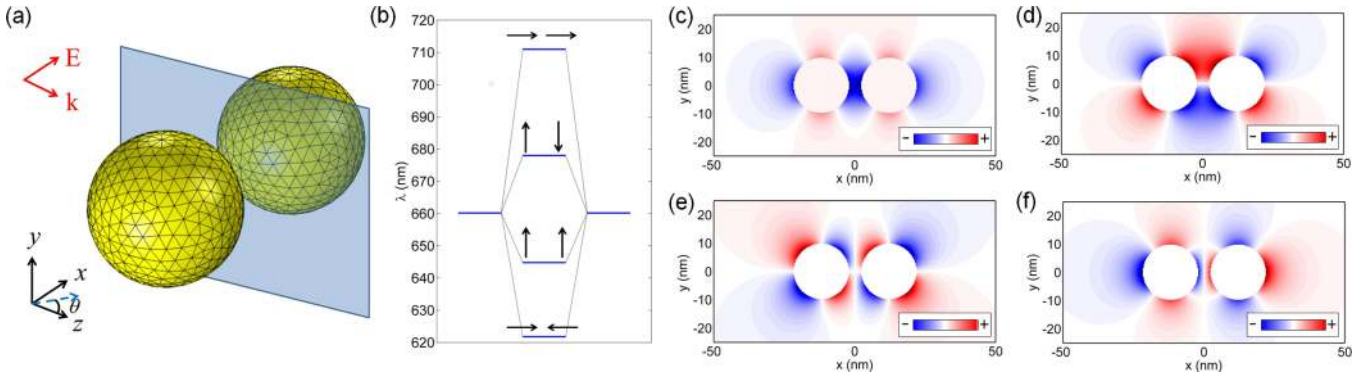

FIG. 1. (Color online) (a) The symmetric gold nanodimers studied in this work. The nanoparticle diameter is 20 nm, and the spacing is 4 nm. The blue plane corresponds to the plane discussed in the main text ($x = 0$). This plane is alternatively a symmetry or antisymmetry plane for the electromagnetic field (see the discussion in the main text). The excitation conditions and the mesh used for the SIE computations are also shown. The scattering angle θ is defined relatively to the z axis. (b) Diagram describing the resonant wavelength of the eigenmodes arising from the coupling between the dipolar modes of two 20 nm gold nanoparticles with a nanogap of 4 nm. The arrows indicate the orientation of the dipolar moments for the corresponding eigenmodes. (c)–(f) Normalized real part of the x-component of the electric field evaluated for the eigenmode with a resonant wavelength of (c) $\lambda = 711$ nm, (d) $\lambda = 678$ nm, (e) $\lambda = 645$ nm, and (f) $\lambda = 622$ nm.

and the SIE method for complete electromagnetic computations. Our approach is the following. The eigenmodes are first characterized; i.e., their resonant wavelengths and their symmetry properties are determined. In order to understand the role played by the different modes in the nonlinear response of the nanoparticle clusters, the exact computations of the SHG are then analyzed, keeping in mind the information provided by the eigenmode analysis. Dispersive gold dielectric constants used for the SIE computation are obtained from experimental data of Johnson and Christy [66]. All the SIE and eigenmode computations are performed for nanoparticle clusters embedded in a high-refractive-index background ($\varepsilon_m = 6.145$ corresponding to TiO_2) in order to shift the surface plasmon resonances away from the interband transition of gold ($\lambda \sim 500$ nm). Symmetric and asymmetric dimers are discussed first (Sec. III A and III B); the case of linear trimers is then investigated in Sec. III C.

A. Symmetric dimer

Let us first consider a dimer of two identical gold nanoparticles with 20 nm diameters. The spacing between the nanoparticles is 4 nm [Fig. 1(a)]. The plasmon resonance for each individual nanoparticle occurs at $\lambda = 660$ nm. Figure 1(b) shows the resonant wavelengths for the different eigenmodes arising from the hybridization between the dipolar modes sustained by the individual nanoparticles. The arrows indicate the orientation of the dipolar moment in each nanoparticle. The total number of eigenmodes is 6, corresponding to 4 resonant wavelengths, since some modes are degenerate ($\lambda = 678$ nm and 645 nm). The degenerate modes have identical dipole moments, but the dipoles are aligned along either the y axis or the z axis. The eigenmode with the longest resonant wavelength ($\lambda = 711$ nm) corresponds to the coupling between two aligned dipole moments pointing in the same direction. On the contrary, the eigenmode with the shortest resonant wavelength ($\lambda = 622$ nm) corresponds to the coupling between two aligned dipole moments pointing in opposite directions. The two other modes correspond to the symmetric and antisymmetric coupling between the dipoles but with the dipoles oriented perpendicular to the axis joining both nanoparticles and parallel to the symmetry plane shown in Fig. 1(a). In other words, the different eigenmodes result from the coupling between the individual dipole modes with different relative orientations. As a consequence, the symmetry properties are different for each mode. The SIE method permits computation of the SH electromagnetic fields, and the comparison with the eigenmode calculations is straightforward when calculating the distribution of the electric field associated with each mode. For this reason, we sort the modes by considering the symmetry of their electric field. The real part of the x-component of the electric field evaluated with the *ab initio* method for the four eigenmodes is shown in Figs. 1(c)–1(f). The x-component corresponds to the vector component normal to the plane shown in Fig. 1(a). The eigenmodes fall into two categories, depending on the symmetry of the electric field with respect to the symmetry plane shown in Fig. 1(a). The two modes with the longest resonant wavelength are defined as antisymmetric modes, since the plane shown in Fig. 1 is an antisymmetry plane (similar to a perfect electric conductor [67]) for these modes [Figs. 1(c) and 1(d)]. The two modes with the shortest resonant wavelength are defined as symmetric modes [Figs. 1(e) and 1(f)]. Indeed, the normal component of the electric field associated with these modes vanishes in the plane $x = 0$, indicating that this plane is a symmetry plane (similar to a perfect magnetic conductor [67]) for these mode.

To investigate the link between the eigenmodes supported by a plasmonic nanostructure and its SH response, let us first consider the excitation of the symmetric nanodimer by an incoming plane wave. SIE computations have been performed with an incident plane wave polarized along the x axis and propagating along the z axis [Fig. 1(a)]. The incident wavelength is $\lambda = 1244$ nm. The near-field distributions of the intensity and the real part of the x-component of the electric field are shown in Figs. 2(a) and 2(c), respectively. It is obvious that these distributions correspond to that of the mode with a resonant wavelength equal to $\lambda = 711$ nm, demonstrating that this mode is excited in this case [compare

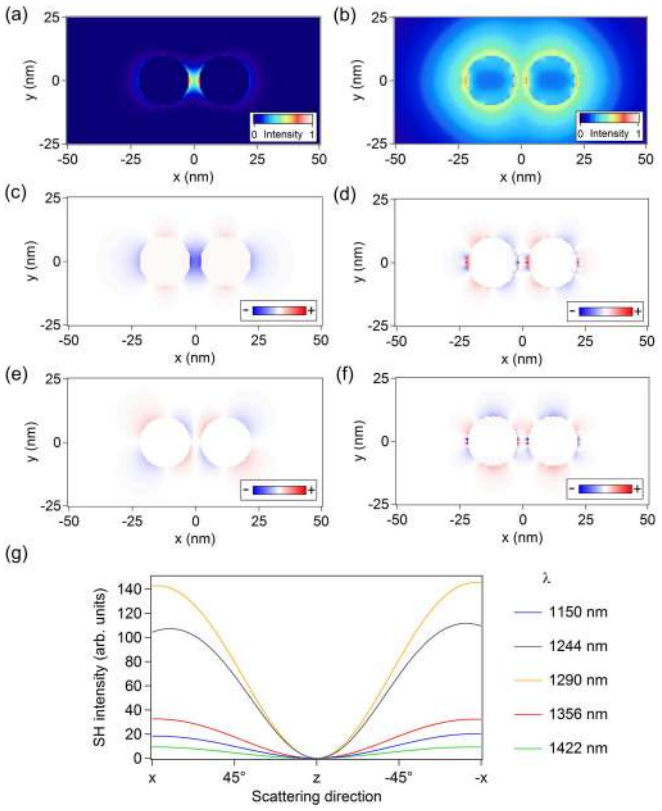

FIG. 2. (Color online) Near-field distribution of (a) the fundamental and (b) the SH intensities close to a nanodimer composed of two 20 nm gold nanoparticles. The spacing between the two nanoparticles is 4 nm. The incident wavelength is $\lambda = 1244$ nm. Real part of the x-component for (c) the fundamental and (d) the SH electric fields, as well as the real part of the z-component for (e) the fundamental and (f) the SH electric fields. (g) Scattered SH intensity as a function of the scattering direction θ (Fig. 1) computed for different incident wavelengths increasing from $\lambda = 1150$ nm to 1422 nm.

Fig. 2(c) with Fig. 1(c)]. Obviously, the incident wavelength used in the SIE calculation ($\lambda = 1244$ nm) does not match the resonance wavelength of the $\lambda = 711$ mode; still, only this mode fulfills the symmetry selection rules imposed by both the cluster geometry and the incident beam properties. Hence, this excitation scheme corresponds to off-resonant excitation, which is of course weaker than in the resonant case (let us recall that the excitation of a Lorentzian mode does not require an exact match between the excitation wavelength and the resonance wavelength, although the excitation is strongest in that, on-resonant, case) [68]. The near-field distribution in Fig. 2(a) is mainly characterized by a significant enhancement of the electric field in the nanogap, where it reaches 30 times the illumination intensity. The intensity enhancement evolves from 25 for an incident wavelength $\lambda = 1422$ nm to 36 for an incident wavelength $\lambda = 1150$ nm. This hotspot is induced by charges with opposite signs standing on each side of the nanogap and is characteristic of the linear response of metallic nanoantennas [69].

Now we turn our attention to the SHG from this nanodimer. Figure 2 shows the SH near-field intensity [panel (b)] as well as the real part of the x- [panel (d)] and z-components [panel (f)] of the SH electric field computed with the SIE. It is obvious that these distributions differ from the ones obtained for the fundamental wave. For instance, the SH field is not enhanced in the nanogap, as is the case for the fundamental field [70]. Contrary to the fundamental electric field, which is driven by an incident plane wave, the SH electric field is driven by the nonlinear polarization sources located at the nanoparticle surfaces. The nonlinear polarization can be expressed as [40]:

$$P_{\perp}(\vec{r},2\omega) = \chi_{S,\perp\perp\perp}\hat{r}(\hat{r}\cdot\vec{E}(\vec{r},\omega))^2, \quad \forall \vec{r} \in S, \tag{6}$$

where $\vec{E}(\vec{r})$ is the fundamental electric field evaluated in the metallic nanoparticle, just below the surface S, and $\hat{r}$ is the outward vector normal to the surface. The following relations are deduced from the properties of the near-field at the fundamental wavelength [see Figs. 2(c) and 2(e)], and the expression of the nonlinear polarization, Eq. (6):

$$P_x(\vec{r}_1,2\omega) = -P_x(\vec{r}_2,2\omega), \tag{7}$$

$$P_{y,z}(\vec{r}_1,2\omega) = P_{y,z}(\vec{r}_2,2\omega), \tag{8}$$

where $\vec{r}_1 = (x,y,z)$ and $\vec{r}_2 = (-x,y,z)$ are linked by a mirror symmetry relation. Note that these relations can be directly deduced from the cluster geometry and the incident wave properties. Since the nonlinear polarization is the physical origin of the SH electric field, the SH electric field must follow the selection rules that apply to the nonlinear polarization, i.e., the rules induced by Eqs. (7) and (8), in order to fulfill the Curie dissymmetry principle. That clearly means that the SH electric field distribution must be described using only symmetric modes, corresponding to the modes for which

$$E_x(\vec{r},2\omega) = 0, \quad \forall \vec{r} = (0,y,z). \tag{9}$$

In other words, only the modes for which the normal component of the electric field vanishes in the plane $x = 0$ have to considered to expand the SH wave. From the eigenmode analysis, it is clear that the two modes with the shortest resonant wavelengths are involved in the SH wave due to their symmetry properties. In order to confirm this hypothesis, the SH intensity scattered in the (O, x, z) plane was calculated as a function of the scattering direction θ [Fig. 2(g)]. Several incident wavelengths, corresponding to the resonant excitation of the eigenmodes at the SH wavelength, were considered in order to determine which modes are active at the SH emission step. Note that the SH intensity vanishes in the forward direction, as expected for a metallic nanostructure with a centrosymmetric shape [40]. The scattered SH intensity is maximal when the symmetric modes are resonantly excited at the SH wavelength, especially the mode corresponding to two parallel dipole moments pointing in the same direction. As discussed by Dadap *et al.* [40] in the case of isolated spherical nanoparticles, this mode is excited by the phase variation of the incident wave across the considered nanostructure. This mode is resonant at $\lambda = 645$ nm and is resonant at the SH wavelength for an incident wavelength $\lambda = 1290$ nm (yellow curve). Indeed, it was shown that localized surface plasmon resonances can increase SHG either at the fundamental or SH wavelength [40]. In this case, the far-field SH intensity is seven times higher than in the off-resonant case ($\lambda =$ 1150 nm), even though the fundamental intensity is slightly

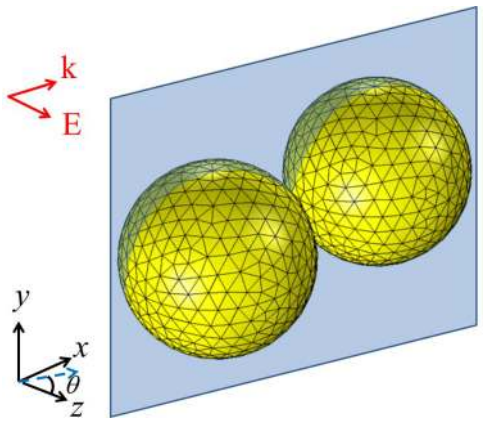

FIG. 3. (Color online) The symmetric gold nanodimers studied in this work. The nanoparticle diameter is 20 nm, and the spacing is 4 nm. The blue plane corresponds to the plane discussed in the main text ($z = 0$). Contrary to Fig. 2, an incident plane wave propagating along the x axis and polarized along the z axis is considered. The scattering angle θ is defined relative to the z axis.

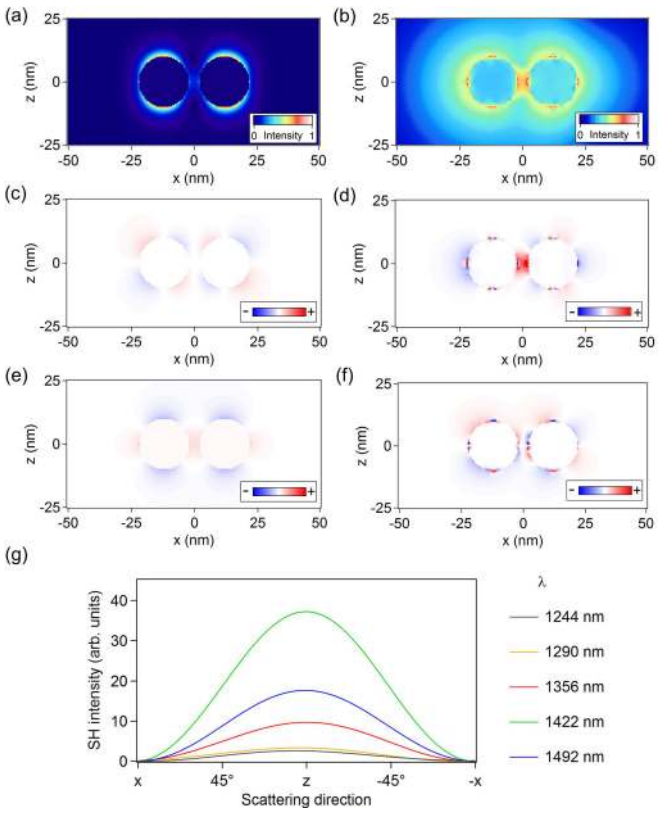

FIG. 4. (Color online) Near-field distribution of (a) the fundamental and (b) the SH intensities close to a nanodimer composed of two 20 nm gold nanoparticles. The spacing between the two nanoparticles is 4 nm. An incident plane wave propagating along the x axis and polarized along the z axis is considered. The incident wavelength is $\lambda = 1244$ nm. Real part of the x-component for (c) the fundamental and (d) the SH electric fields, as well as the real part of the z-component for (e) the fundamental and (f) the SH electric fields. (g) Scattered SH intensity as a function of the scattering direction θ (Fig. 3) computed for different incident wavelengths increasing from $\lambda = 1244$ nm to 1492 nm.

lower. This observation indicates that the symmetric modes are the ones involved in the scattered SH wave, as predicted by the eigenmode analysis. These results indicate that modes with the required symmetry properties effectively contribute to the SHG from coupled plasmonic nanostructures, although these modes cannot be directly excited by an incoming plane wave in the linear regime.

B. Influence of the excitation condition

In order to investigate the influence of the excitation condition on the derived selection rules, an incident plane wave propagating along the x axis and polarized along the z axis is considered (see Fig. 3). The first consequence of this excitation configuration is that the plane $x = 0$ is no longer a symmetry/antisymmetry plane. In the present case, the selection rules must be derived relative to the plane $z = 0$ (Fig. 3) and can be written as:

$$P_z(\vec{r}_1,2\omega) = -P_z(\vec{r}_2,2\omega), \tag{10}$$

$$P_{x,y}(\vec{r}_1,2\omega) = P_{x,y}(\vec{r}_2,2\omega), \tag{11}$$

where $\vec{r}_1 = (x,y,z)$ and $\vec{r}_2 = (x,y,-z)$ are linked by a mirror symmetry relation, and

$$E_z(\vec{r},2\omega) = 0, \quad \forall \vec{r} = (x,y,0). \tag{12}$$

The plane $z = 0$ is clearly an antisymmetry plane for the fundamental electric field but a symmetry one for the SH electric field (see the near-field distributions in Fig. 4), as observed for the plane $x = 0$ when an incident plane wave polarized along the x axis and propagating along the z axis is considered (see the discussion in Sec. III A). The mode excited

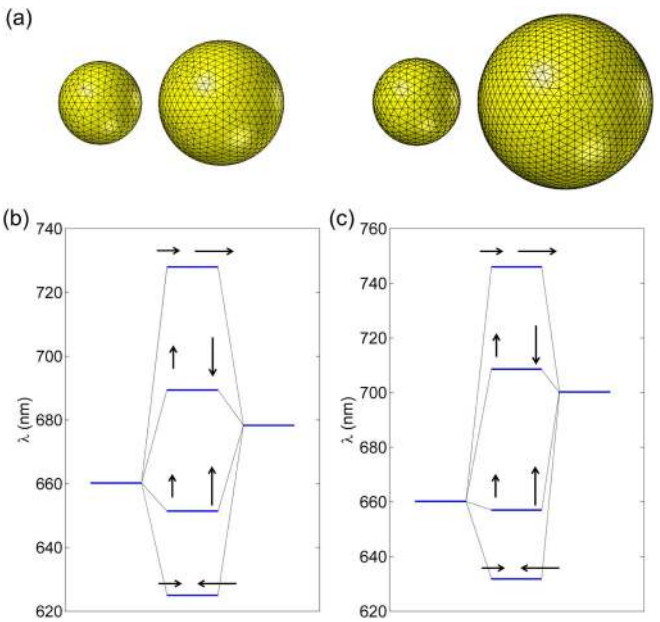

FIG. 5. (Color online) (a) The two asymmetric nanodimers considered in this work. Diagrams describe the resonant wavelength of the eigenmodes arising from the coupling between the dipolar modes of an asymmetric dimer composed of a 20 nm gold nanoparticle with (b) a 30 nm or (c) a 40 nm gold nanoparticle. The spacing between the two nanoparticles is 4 nm.

at the fundamental wavelength is the one for which two parallel dipole moments point in the same direction [see Fig. 1(e)]. The mode excited at the SH wavelength corresponds to the mode for which two aligned dipole moments point in the same direction [see Fig. 1(c)]. This observation is confirmed by the far-field analysis. Indeed, the far-field SH intensity is maximal when this mode is resonantly excited at the SH wavelength [Fig. 4(g)], demonstrating that the contribution of this mode to the scattered SH wave is important. It is interesting to note that here the excitation scheme is the reverse of the previous one: The mode excited at the fundamental (SH) wavelength in the previous case is now the mode excited at the SH (fundamental) wavelength. Nevertheless, the far-field SH intensity vanishes along the backward and forward directions in each case. In the following part, asymmetric dimers are considered, reducing the symmetry of the problem under study in order to test the generality of the derived selection rules and to address the influence of symmetry breaking on the SH response of nanoparticle clusters.

C. Asymmetric dimers

Dimers composed of gold nanoparticles with different diameters are investigated. Similar systems were experimentally studied [71]. The diameter of one nanoparticle is kept constant (20 nm) while two different diameters are considered for the second, larger, nanoparticle: 30 nm and 40 nm. These nanodimers are no longer centrosymmetric [Fig. 5(a)]. The nanogap is 4 nm for all cases. The plasmon resonance wavelength for the 30 nm nanoparticle is $\lambda = 678$ nm and that of the 40 nm nanoparticle is $\lambda = 700$ nm. Figure 5 shows the wavelengths of the eigenmodes arising from the coupling between the dipolar modes of a 20 nm gold nanoparticle with the dipolar modes of a 30 nm [Fig. 5(b)] or a 40 nm [Fig. 5(c)] gold nanoparticle. The resonance wavelengths of the hybridized modes, as compared to the symmetric dimer, are different, since the resonance wavelengths of the individual dipole modes supported by the nanoparticles vary with the nanoparticle diameter. Nevertheless, the orientations of the dipolar moment for the different hybridized modes are identical to those of the symmetric dimer discussed in Sec. III A. For instance, for all the nanodimers studied, the hybridized mode with the longest resonant wavelength corresponds to the coupling between two dipolar moments aligned in the same direction. The near-field distributions of the fundamental and SH intensities, as well as the corresponding distribution of the real part of the x-component of the electric field, were computed using SIE for an incident plane wave

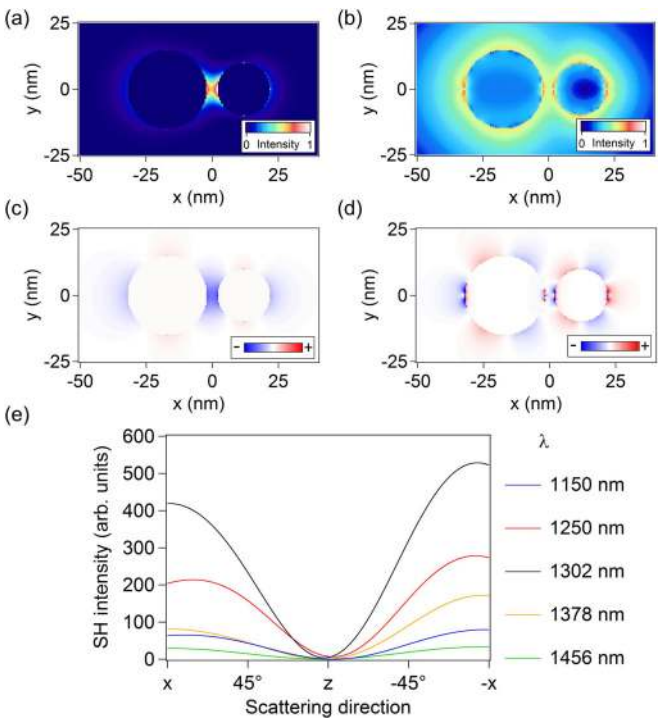

FIG. 6. (Color online) Near-field distribution for (a) the fundamental and (b) the SH intensities close to a nanodimer composed of a 20 nm and a 30 nm gold nanoparticle. The spacing between the two nanoparticles is 4 nm. The incident wavelength is 1456 nm. Real part of the x-component for (c) the fundamental and (d) the SH electric fields. (e) Scattered SH intensity as a function of the scattering direction computed for fundamental wavelengths increasing from $\lambda = 1150$ nm to $\lambda = 1456$ nm.

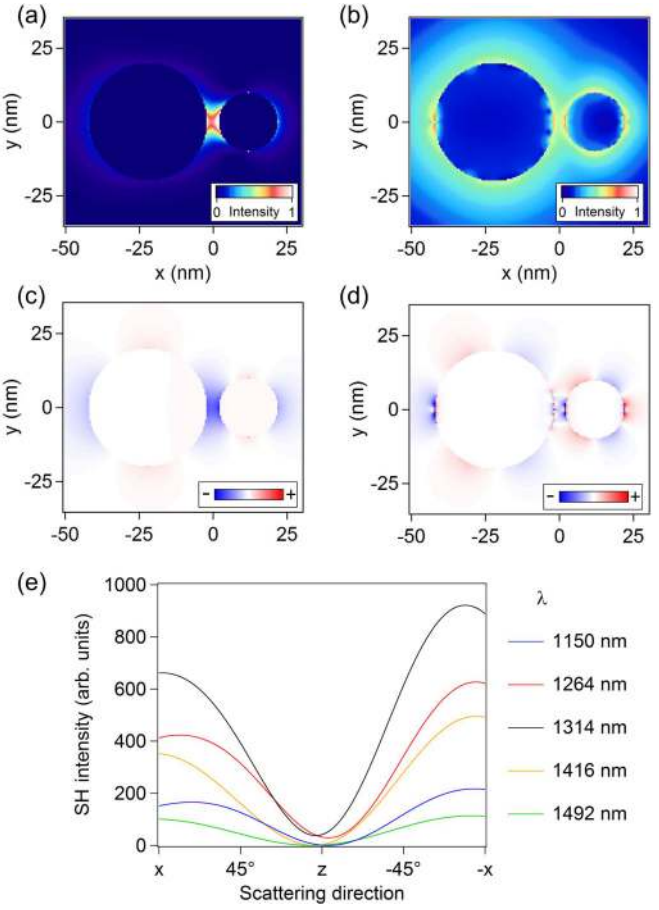

FIG. 7. (Color online) Near-field distribution for (a) the fundamental and (b) the SH intensities close to a nanodimer composed of a 20 nm and a 40 nm gold nanoparticle. The spacing between the two nanoparticles is 4 nm. The incident wavelength is $\lambda = 1492$ nm. Real part of the x-component for (c) the fundamental and (d) the SH electric fields. (e) Scattered SH intensity as a function of the scattering direction computed for fundamental wavelengths increasing from $\lambda = 1150$ nm to $\lambda = 1492$ nm.

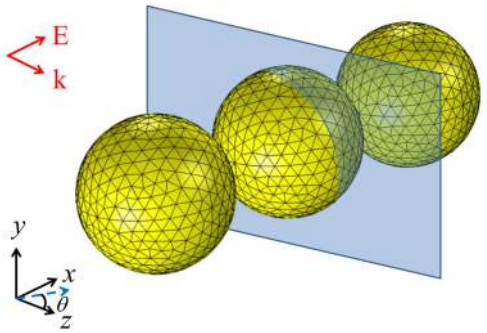

FIG. 8. (Color online) The gold nanotrimers studied in this work. The nanoparticle diameter is 20 nm, and the spacing is 4 nm. The blue plane corresponds to the plane discussed in the main text ($x = 0$). This plane is alternatively a symmetry or antisymmetry plane for the electromagnetic field (see the discussion in the main text). The scattering angle θ is defined relative to the z axis.

polarized along the x axis and propagating along the z axis (see Figs. 6 and 7). At the first sight, the general behavior of the near-field distributions is identical to that observed for the symmetric nanodimer. For example, an enhancement of the fundamental electric field is observed in the nanogap, but no particular enhancement of the SH electric field in this region is visible [Figs. 6(b) and 7(b)]. This observation indicates that the selection rules derived in the previous section are qualitatively followed in the case of asymmetric dimers, even though these nanostructures do not possess any symmetry/antisymmetry planes. Note that the nanoparticles considered in the present work are perfectly spherical, but the selection rules are broken in the case of realistic metallic nanoparticles with small sizes, as was experimentally demonstrated [72]. In order to investigate the influence of the asymmetry on the SHG in the far-field, the SH intensity scattered in the (O, x, z) plane was calculated as a function of the scattering direction for the two asymmetric nanodimers considering several incident wavelengths corresponding to resonant excitation of the eigenmodes at the SH wavelength (see Fig. 5). As in the case of the symmetric nanodimer, the scattered SH intensity is maximal when the symmetric modes (using the same terminology even though the field amplitudes are different in the asymmetric cases; Figs. 6 and 7) are resonantly excited at the SH wavelength. The asymmetry of the nanodimer is clearly revealed by the SH far-field, since the SH intensity scattered along the $-x$ direction differs from that scattered along the x direction [Figs. 6(e) and 7(e)] [36]. Even though the centrosymmetry is broken, the SH intensity scattered in the forward direction is not dramatically increased but remains only a small part of the total SH intensity. This observation is consistent with previous experimental results, which report lower SHG from asymmetric dimers than from symmetric ones [71]. This point confirms that the selection rules are not completely broken when the diameter of one of the nanoparticles is twice the diameter of the other one.

D. Linear trimer

Metallic nanostructures with several nanogaps are also promising for applications in nonlinear plasmonics. For

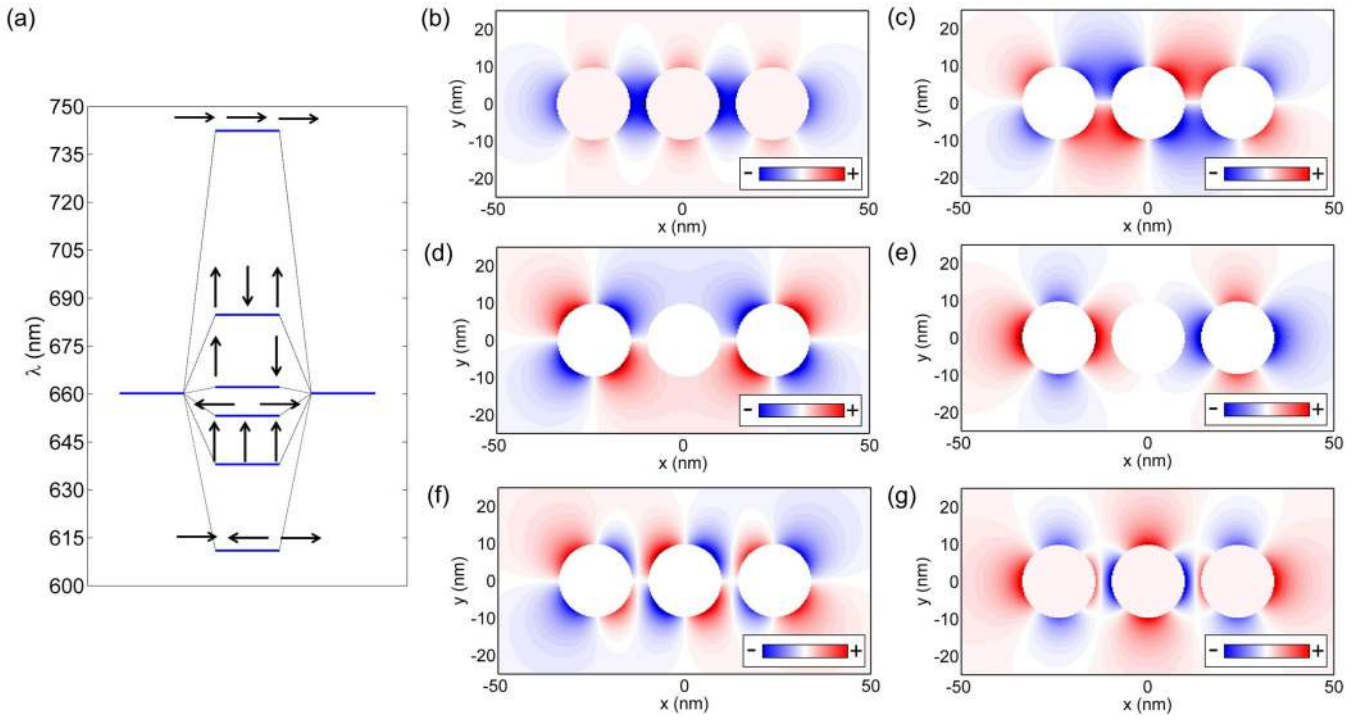

FIG. 9. (Color online) (a) Diagram describing the resonant wavelength of the eigenmodes arising from the coupling between the dipolar modes of three 20 nm gold nanoparticles with nanogaps of 4 nm. The three nanoparticles are lined up along the x axis. The arrows indicate the orientation of the dipolar moments for the corresponding eigenmodes. (b)–(g) Real part of the x-component of the electric field evaluated for the eigenmode with a resonant wavelength of (b) 742.5 nm, (c) 685 nm, (d) 662 nm, (e) 653 nm, (f) 638 nm, and (g) 611 nm.

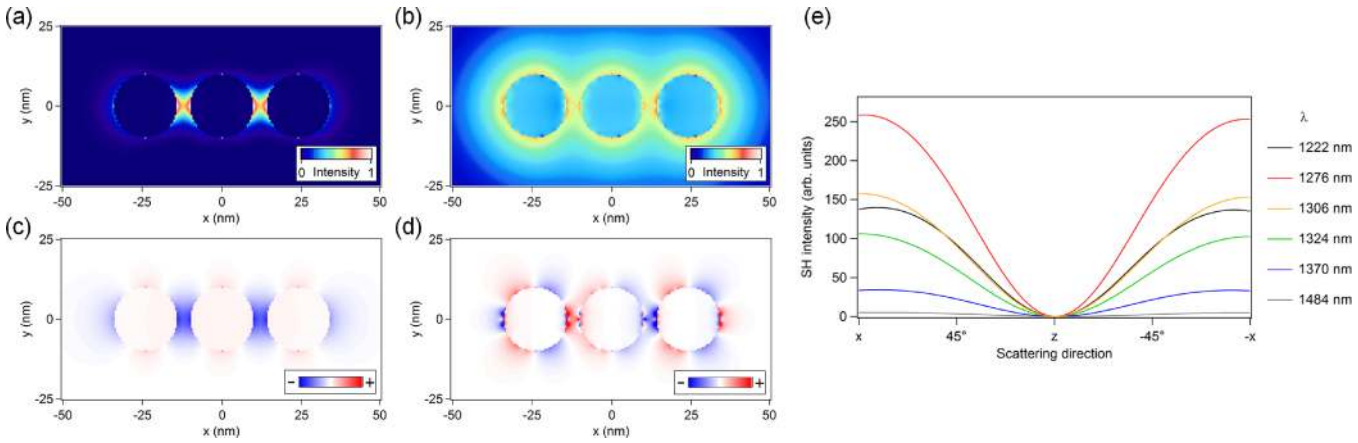

FIG. 10. (Color online) Near-field distribution of (a) the fundamental and (b) the SH intensities close to a linear nanotrimer composed of three 20 nm gold nanoparticles. The spacing between the nanoparticles is 4 nm. The incident wavelength is $\lambda = 1306$ nm. Real part of the x-component for (c) the fundamental and (d) the SH electric fields. (e) The scattered SH intensity as a function of the scattering direction computed for incident wavelength increasing from $\lambda = 1222$ nm to $\lambda = 1484$ nm.

example, it was recently demonstrated that the SHG from three-arm multiresonant plasmonic nanoantennas is higher than SHG from antennas resonant only at the fundamental wavelength [73]. A linear nanotrimer composed of three identical 20 nm nanoparticles lined up with 4 nm separations is considered (Fig. 8). The eigenmode analysis for this cluster is presented in Fig. 9. The total number of eigenmodes is nine, corresponding to six resonant wavelengths, since modes with resonant wavelengths $\lambda = 685$ nm, 662 nm, and 638 nm are degenerated. As observed in the case of the symmetric nanodimer studied in Sec. III A, both symmetric and antisymmetric modes resulting from the coupling between original dipolar modes are revealed by the eigenmode analysis. SIE computations were performed considering an incident plane wave polarized along the x axis and propagating along the z axis. Due to the specific nanoparticles' organization and fundamental near-field distribution symmetry (Fig. 10), the selection rules [Eqs. (7) and (8)] derived for the SHG from symmetric nanodimer also apply to the case of SHG from this linear nanotrimer. Note that the x-component of the SH electric field does not necessary vanish in the gap center, since the nanogaps do not stand in the $x = 0$ plane (the symmetry plane shown in Fig. 8). Indeed, the fundamental electric field amplitudes computed on each side of a given nanogap are not perfectly identical, and the amplitudes of the nonlinear currents are then different, which does not result in total destructive interferences. In order to determine which modes dominate the nonlinear response, the SH intensity scattered in the (O, x, z) plane was calculated as a function of the scattering direction and shown in Fig. 10(e). Several incident wavelengths, corresponding to resonant excitation of the available eigenmodes at the SH wavelength, were considered. As observed in the case of the nanodimers, the SH far-field intensity is maximal when the SH wavelength matches the resonant wavelength of the mode for which all the dipolar moments are parallel and pointing in the same direction. This confirms that the derived selection rules are general and can be applied to different kinds of nanoparticle clusters.

IV. CONCLUSIONS

In summary, SHG from interacting spherical plasmonic nanoparticles was theoretically investigated comparing an *ab initio* approach based on the Green's functions method with the SIE method. Several cluster geometries, including symmetric/asymmetric dimers, and linear trimers, were considered in this work. The fundamental and SH responses of the corresponding clusters were computed, and an eigenmode analysis was performed. The role played by the different eigenmodes in the SHG, at both the excitation and reemission steps, was emphasized in relation to the cluster symmetry. It was in particular observed that the SHG can be significantly enhanced when the fundamental field is such that its SH matches modes with suitable symmetry. The results presented in this article are not specific to SHG. Our method can be applied to complex assemblies with an arbitrary number of nanoparticles, as well as other nonlinear optical processes, such as third-harmonic generation. However, the method used in this work for the determination of the eigenmodes only involves the dipolar modes supported by the individual nanoparticles, while in specific cases, higher multipolar modes should be included to obtain a complete description of wave-mixing processes from nanoparticle assemblies, as underlined in the case of SHG [40,74]. In order to handle such higher multipolar modes as well as the influence of a dielectric substrate on the eigenmode properties, an electrostatic eigenmode method was developed and represents a useful approach to complement the exact electromagnetic computations presented here for fully understanding and tailoring the nonlinear response of coupled metallic nanoparticles [75–79].

ACKNOWLEDGMENTS

Funding from the Swiss National Science Foundation (Project No. 200020_153662) is gratefully acknowledged.

[1] W. L. Barnes, A. Dereux, and T. W. Ebbesen, Nature **424**, 824 (2003).

[2] S. A. Maier, in *Plasmonics: Fundamentals and Applications* (Springer, New York, 2007).

[3] A. Crut, P. Maioli, N. Del Fatti, and F. Vallée, Chem. Soc. Rev. **43**, 3921 (2014).

[4] K. L. Kelly, E. Coronado, L. L. Zhao, and G. C. Schatz, J. Phys. Chem. B **107**, 668 (2003).

[5] L. J. Sherry, S.-H. Chang, G. C. Schatz, R. P. Van Duyne, B. J. Wiley, and Y. Xia, Nano Lett. **5**, 2034 (2005).

[6] B. Gallinet and O. J. F. Martin, ACS Nano **7**, 6978 (2013).

[7] A. Campion and P. Kambhampati, Chem. Soc. Rev **27**, 241 (1998).

[8] S. M. Nie and S. R. Emery, Science **275**, 1102 (1997).

[9] K. Kneipp, Y. Wang, H. Kneipp, L. T. Perelman, I. Itzkan, R. R. Dasari, and M. S. Feld, Phys. Rev. Lett. **78**, 1667 (1997).

[10] N. J. Halas, S. Lal, W.-S. Chanq, S. Link, and P. Nordlander, Chem. Rev. **111**, 3913 (2011).

[11] E. Prodan, C. Radloff, N. J. Halas, and P. Nordlander, Science **302**, 419 (2003).

[12] K.-H. Su, Q.-H. Wei, X. Zhang, J. J. Mock, D. R. Smith, and S. Schultz, Nano Lett. **3**, 1087 (2003).

[13] T. Atay, J.-H. Song, and A. V. Nurmikko, Nano Lett. **4**, 1627 (2004).

[14] J. P. Kottmann and O. J. F. Martin, Opt. Express **8**, 655 (2001).

[15] P. K. Jain, W. Huang, and M. A. El-Sayed, Nano Lett. **7**, 2080 (2007).

[16] B. Luk'yanchuk, N. I. Zheludev, S. A. Maier, N. J. Halas, P. Nordlander, H. Giessen, and C. T. Chong, Nat. Mater. **9**, 707 (2010).

[17] B. Gallinet and O. J. Martin, ACS Nano **5**, 8999 (2011).

[18] M. Rahmani, D. Y. Lei, V. Giannini, B. Luk'yanchuck, M. Ranjbar, T. Y. F. Liew, M. H. Hong, and S. A. Maier, Nano Lett. **12**, 2101 (2012).

[19] L. Chuntonov and G. Haran, Nano Lett. **11**, 2440 (2011).

[20] D. E. Gómez, Z. Q. Teo, M. Altissimo, T. J. Davis, S. Earl, and A. Roberts, Nano Lett. **13**, 3722 (2013).

[21] J. A. Fan, K. Bao, C. Wu, J. Bao, R. Bardhan, N. J. Halas, V. N. Manoharan, G. Shvets, P. Nordlander, and F. Capasso, Nano Lett. **10**, 4680 (2010).

[22] F. Shafiei, F. Monticone, K. Q. Le, X.-X. Liu, T. Hartsfield, A. Alù, and X. Li, Nature Nanotechnology **8**, 95 (2013).

[23] M. Hentschel, M. Saliba, R. Vogelgesang, H. Giessen, A. P. Alivisatos, and N. Liu, Nano Lett. **10**, 2721 (2010).

[24] N. A. Mirin, K. Bao, and P. Nordlander, J. Phys. Chem. A **113**, 4028 (2009).

[25] W. Zhang, B. Gallinet, and O. J. F. Martin, Phys. Rev. B **81**, 233407 (2010).

[26] A. Bouhelier, M. Beversluis, A. Hartschuh, and L. Novotny, Phys. Rev. Lett. **90**, 013903 (2003).

[27] B. K. Canfield, H. Husu, J. Laukkanen, B. F. Bai, M. Kuittinen, J. Turunen, and M. Kauranen, Nano Lett. **7**, 1251 (2007).

[28] J. Butet, J. Duboisset, G. Bachelier, I. Russier-Antoine, E. Benichou, C. Jonin, and P.-F. Brevet, Nano Lett. **10**, 1717 (2010).

[29] Y. Zhang, N. K. Grady, C. Ayala-Orozco, and N. J. Halas, Nano Lett. **11**, 5519 (2011).

[30] M. Lippitz, M. A. van Dijk, and M. Orrit, Nano Lett. **5**, 799 (2005).

[31] M. Hentschel, T. Utikal, H. Giessen, and M. Lippitz, Nano Lett. **12**, 3778 (2012).

[32] H. Harutyunyan, G. Volpe, R. Quidant, and L. Novotny, Phys. Rev. Lett. **108**, 217403 (2012).

[33] J. Butet, I. Russier-Antoine, C. Jonin, N. Lascoux, E. Benichou, and P.-F. Brevet, Nano Lett. **12**, 1697 (2012).

[34] J. Butet and O. J. F. Martin, ACS Nano **8**, 4931 (2014).

[35] G. Bautista, M. J. Huttunen, J. Mäkitalo, J. M. Kontio, J. Simonen, and M. Kauranen, Nano. Lett. **12**, 3207 (2012).

[36] J. Butet, K. Thyagarajan, and O. J. F. Martin, Nano Lett. **13**, 1787 (2013).

[37] C. Sauerbeck, M. Haderlein, B. Schürer, B. Braunschweig, W. Peukert, and R. N. K. Taylor, ACS Nano **8**, 3088 (2014).

[38] H. Harutyunyan, S. Palomba, J. Renger, R. Quidant, and L. Novotny, Nano Lett. **10**, 5076 (2010).

[39] V. K. Valev, Langmuir **28**, 15454 (2012).

[40] J. I. Dadap, J. Shan, and T. F. Heinz, J. Opt. Soc. Am. B **21**, 1328 (2004).

[41] C. C. Neacsu, G. A. Reider, and M. B. Raschke, Phys. Rev. B **71**, 201402(R) (2005).

[42] M. Finazzi, P. Biagioni, M. Celebrano, and L. Duò, Phys. Rev. B **76**, 125414 (2007).

[43] P. Ginzburg, A. Krasavin, Y. Sonnefraud, A. Murphy, R. J. Pollard, S. A. Maier, and A. V. Zayats, Phys. Rev. B **86**, 085422 (2012).

[44] Y. Zeng, D. A. R. Dalvit, J. O'Hara, and S. A. Trugman, Phys. Rev. B **85**, 125107 (2012).

[45] J. Xu and X. Zhang, Opt. Express **20**, 1668 (2012).

[46] A. Rose, D. Huang, and D. R. Smith, Phys. Rev. Lett. **110**, 063901 (2013).

[47] Y. Liu and X. Zhang, Phys. Rev. A **88**, 063810 (2013).

[48] G. Bachelier, I. Russier-Antoine, E. Benichou, C. Jonin, and P.-F. Brevet, J. Opt. Soc. Am. B **25**, 955 (2008).

[49] J. Mäkitalo, S. Suuriniemi, and M. Kauranen, Opt. Express **19**, 23386 (2011).

[50] Y. Zeng, W. Hoyer, J. J. Liu, S. W. Koch, and J. V. Moloney, Phys. Rev. B **79**, 235109 (2009).

[51] M. Scalora, M. A. Vincenti, D. de Ceglia, V. Roppo, M. Centini, N. Akozbek, and M. J. Bloemer, Phys. Rev. A **82**, 043828 (2010).

[52] J. Butet, I. Russier-Antoine, C. Jonin, N. Lascoux, E. Benichou, O. J. F. Martin, and P.-F. Brevet, Phys. Rev. B **87**, 235437 (2013).

[53] K. Thyagarajan, J. Butet, and O. J. F. Martin, Nano Lett. **13**, 1847 (2013).

[54] Y. Zhang, F. Wen, Y. R. Zhen, P. Nordlander, and N. J. Halas, PNAS **110**, 9215 (2013).

[55] O. J. F. Martin and N. B. Piller, Phys. Rev. E **58**, 3909 (1998).

[56] M. A. Yurkin and M. Kahnert, J. Quant. Spectrosc. Radiat. Transfer **123**, 176 (2013).

[57] P. G. Etchegoin, E. C. Le Ru, and M. Meyer, J. Chem. Phys. **125**, 164705 (2006).

[58] J. Mäkitalo, M. Kauranen, and S. Suuriniemi, Phys. Rev. B **89**, 165429 (2014).

[59] J. Butet, B. Gallinet, K. Thyagarajan, and O. J. F. Martin, J. Opt. Soc. Am. B **30**, 2970 (2013).

[60] S. Rao, D. Wilton, and A. Glisson, IEEE Trans. Antennas Propag. **30**, 409 (1982).

[61] A. M. Kern and O. J. F. Martin, J. Opt. Soc. Am. A **26**, 732 (2009).

[62] G. Bachelier, J. Butet, I. Russier-Antoine, C. Jonin, E. Benichou, and P.-F. Brevet, Phys. Rev. B **82**, 235403 (2010).
[63] F. X. Wang, F. J. Rodriguez, W. M. Albers, R. Ahorinta, J. E. Sipe, and M. Kauranen, Phys. Rev. B **80**, 233402 (2009).
[64] T. F. Heinz, in *Nonlinear Surface Electromagnetic Phenomena*, edited by H.-E. Ponath and G. I. Stegeman (Elsevier, Amsterdam, 1991), pp. 353–416.
[65] T. K. Wu and L. L. Tsai, Radio Sci. **12**, 709 (1977).
[66] P. B. Johnson and R. W. Christy, Phys. Rev. B **6**, 4370 (1972).
[67] A. Taflov and S. C. Hagness, in *Computational Electrodynamics: The Finite-Difference Time-Domain Method*, 2nd ed. (Artech House, Boston, 2000).
[68] C. F. Bohren and D. R. Huffman, in *Absorption and Scattering of Light by Small Particles* (Wiley, New York, 1983).
[69] P. Muhlschlegel, H. J. Eisler, O. J. F. Martin, B. Hecht, and D. W. Pohl, Science **308**, 1607 (2005).
[70] J. Berthelot, G. Bachelier, M. Song, P. Rai, G. Colas des Francs, A. Dereux, and A. Bouhelier, Opt. Express **20**, 10498 (2012).
[71] A. Slablab, L. Le Xuan, M. Zielinski, Y. de Wilde, V. Jacques, D. Chauvat, and J.-F. Roch, Opt. Express **20**, 220 (2012).
[72] J. Nappa, G. Revillod, I. Russier-Antoine, E. Benichou, C. Jonin, and P.-F. Brevet, Phys. Rev. B **71**, 165407 (2005).
[73] K. Thyagarajan, S. Rivier, A. Lovera, and O. J. F. Martin, Opt. Express **20**, 12860 (2012).
[74] J. I. Dadap,J. Shan, K. B. Eisenthal, and T. F. Heinz, Phys. Rev. Lett. **83**, 4045 (1999).
[75] I. D. Mayergoyz, D. R. Fredkin, and Z. Zhang, Phys. Rev. B **72**, 155412 (2005).
[76] T. J. Davis, K. C. Vernon, and D. E. Gómez, Phys. Rev. B **79**, 155423 (2009).
[77] D. E. Gómez, K. C. Vernon, and T. J. Davis, Phys. Rev. B **81**, 075414 (2010).
[78] K. C. Vernon, A. M. Funston, C. Novo, D. E. Gómez, P. Mulvaney, and T. J. Davis, Nano Lett. **10**, 2080 (2010).
[79] C. Forestiere, L. Dal Negro, and G. Miano, Phys. Rev. B **88**, 155411 (2013).